Calculations on Nuclear-Transfer Reactions between Heavy Ions*

F. SCHMITTROTH AND W. TOBOCMAN
Physics Department, Case Western Reserve University, Cleveland, Ohio 44106
AND
A. A. GOLESTANEH
Physics and Astronomy Department, Mount Union College, Alliance, Ohio 44601

(Received 9 May 1969; revised manuscript received 10 November 1969)

Finite-range stripping calculations are made for heavy-ion reactions which involve nucleon transfer. Three reactions have been studied, ^{10}B(^{14}N, ^{15}N)^{11}B, ^{27}Al(^{16}O, ^{15}N)^{28}Si, and ^{11}B(^{16}O, ^{15}N)^{12}C, which span energy regions below, near, and above the Coulomb barrier, respectively. At the low energies, there is quantitative agreement with experimental angular distributions and total cross sections. At higher energies, the agreement with experiment deteriorates as the results become more sensitive to the optical-model parameters used in the calculations. The effects of a repulsive core are noted, and attempts are made to fit some ^{16}O–^{11}B elastic scattering data.

I. INTRODUCTION

REACTION cross sections in heavy ions have been studied by several means. These include a semiclassical neutron-tunneling theory,[1] a diffraction theory,[2] and approximate DWBA[3] theories. Based on a method[4] which treats finite-range effects to any desired accuracy, this paper presents DWBA calculations for a number of nucleon-transfer reactions.

Three reactions are examined, ^{10}B(^{14}N, ^{13}N)^{11}B, ^{27}Al(^{16}O, ^{15}N)^{28}Si, and ^{11}B(^{16}O, ^{15}N)^{12}C. Data for these reactions are given in Refs. 5, 6, and 7, respectively. These three cases include incident energies below the Coulomb barrier, comparable to it, and above it. At the low energies, the first reaction proceeds by neutron tunneling, and the results are compared with the tunneling theories. At the higher energies, both the angular distributions and total cross sections become sensitive to the optical-model parameters. Thus a determination of the optical parameters from ^{11}B-^{11}O elastic scattering[8] was attempted. In particular, since there is evidence for a repulsive core in heavy-ion optical potentials,[9] the effect of a core upon both the elastic and reaction angular distributions was examined.

Except for the neglect of certain recoil effects, the calculations are exact within the framework of a DWBA theory. The diffraction theory is based on the DWBA theory and agrees with the tunneling theory at energies below the Coulomb barrier. The results of this paper thus allow an appraisal of the approximations used in the other theories.

II. THEORETICAL EXPRESSIONS

The reactions in this paper are of the form

$$D+I\equiv(P+N)+I\rightarrow P+(N+I)\equiv P+F.$$

D and I represent the initial colliding projectiles, while P and F denote corresponding final nuclei. N is the transferred nucleon. The appropriate DWBA amplitude is[3]

$$A=\langle\Psi_{PF}^{(-)}\chi_P^{J_PM_P}[\chi_N,\chi_I]_F^{J_FM_F}\mid V_{PN}\times\mid\Psi_{DI}^{(+)}\chi_I^{J_IM_I}[\chi_N,\chi_P]_D^{J_DM_D}\rangle. \quad (1)$$

χ_P, χ_N, χ_I represent internal wave functions, including appropriate spin coordinates, for P, N, and I, respectively. $[\chi_N,\chi_P]_D^{J_DM_D}$ represents N bound to P with total angular momentum J_D and z component M_D. $\Psi_{DI}^{(+)}$ is the initial distorted wave with outgoing boundary conditions. The final-state wave functions follow similar conventions. V_{PN} is the interaction between P and N.

$\theta_{j_1l_1}^{(1)}$ and $\theta_{j_2l_2}^{(2)}$ are defined by[3]

$$\langle[\chi_N,\chi_I]_F^{J_FM_F}\mid\chi_I^{J_IM_I}\rangle=\sum_{j_2l_2}\theta_{j_2l_2}^{(2)}(j_2J_Im_2M_I\mid J_FM_F)\langle\phi_{j_2l_2m_2}\mid \quad (2a)$$

and

$$\langle\chi_P^{J_PM_P}\mid[\chi_N,\chi_P]_D^{J_DM_D}\rangle=\sum_{j_1l_1}\theta_{j_1l_1}^{(1)}(j_1J_Pm_1M_P\mid J_DM_D)\mid\phi_{l_1j_1m_1}\rangle. \quad (2b)$$

The ϕ_{ljm}'s are single-particle nucleon wave functions in a j-j coupled representation which represent the trans-

* Work supported by the U.S. Atomic Energy Commission.

[1] G. Breit and M. E. Ebel, Phys. Rev. **103**, 679 (1956).
[2] A. Dar, Phys. Rev. **139**, B1193 (1965).
[3] P. J. A. Buttle and L. J. B. Goldfarb, Nucl. Phys. **78**, 409 (1966); T. L. Abelishvili, Zh. Eksperim. i Teor. Fiz. [English transl.: Soviet Phys.—JETP **13**, 1010 (1961)]; T. Kammuri and R. Nakasima, in *Proceedings of the Third Conference on Reactions Between Complex Nuclei*, edited by A. Ghiorso and H. E. Conzett (University of California Press, Berkeley and Los Angeles, 1963), p. 163.
[4] T. Sawaguri and W. Tobocman, J. Math. Phys. **8**, 2223 (1967).
[5] R. M. Gaedke, K. S. Toth, and I. R. Williams, Phys. Rev. **141**, 996 (1966); J. G. Couch, J. A. McIntyre, and J. C. Hiebert, *ibid.* **152**, 883 (1966).
[6] E. Newman, K. S. Toth, and A. Zucher, Phys. Rev. **132**, 1720 (1963).
[7] R. Bock, M. Grosse-Schulte, W. v. Oertzen, and R. Rüdel, Phys. Letters **18**, 45 (1965).
[8] W. v. Oertzen, R. Bock, and M. Gross-Schulte, Z. Naturforschg. **21a**, 946 (1966).
[9] K. A. Brueckner, J. R. Buchler, and M. M. Kelly, Phys. Rev. **173**, 944 (1968); R. J. Munn, B. Block, and F. B. Malik, Phys. Rev. Letters **21**, 159 (1968).

TABLE I. Reaction quantum numbers and spectroscopic factors.

Reaction (transition)	Spectroscopic factors S_1 S_2 S	Single-particle transition	Orbital-angular-momentum transfer L
^{10}B(^{14}N, ^{13}N)^{11}B	1.×1.1=1.1	$1p_{1/2}\rightarrow 1p_{3/2}$	2
^{27}Al(^{16}O, ^{15}N)^{28}Si (g.s.)	2×6=12	$1p_{1/2}\rightarrow 1d_{5/2}$	3
^{27}Al(^{16}O, ^{15}N)^{28}Si (1.78 MeV)	2×1=2	$1p_{1/2}\rightarrow 2s_{1/2}$	1
^{27}Al(^{16}O, ^{15}N)^{28}Si (1.78 MeV)[a]	2×1=2	$1p_{1/2}\rightarrow 1d_{3/2}$	1
^{11}B(^{16}O, ^{15}N)^{12}C (g.s.)	2×4=8	$1p_{1/2}\rightarrow 1p_{3/2}$	2
^{11}B(^{16}O, ^{15}N*)^{12}C (6.33 MeV)[b]	4×4=16	$1p_{3/2}\rightarrow 1p_{3/2}$	0, 2
^{11}B(^{16}O, ^{12}C)^{15}N* (6.33 MeV)[c]	1×1=1	$1s\rightarrow 1s$	0

[a] Not calculated.
[b] Proton transfer.
[c] α-particle transfer.

ferred nucleon bound to the initial and final nuclei, D and F.

The differential cross section is proportional to

$$X=[(2J_I+1)(2J_D+1)]^{-1}\sum_{M_IM_D,M_PM_F}|A|^2. \quad (3)$$

After some Racah algebra one obtains

$$X=\frac{(2J_F+1)}{(2J_I+1)}\sum_{LM}\frac{(2L+1)}{(2l_1+1)}|\theta_{j_1l_1}{}^{(1)}\theta_{j_2l_2}{}^{(2)}W(l_2j_2l_1j_1;\tfrac{1}{2}L)$$
$$\times\sum_{m_1m_2}(l_2Lm_2M\,|\,l_1m_1)\langle\Psi_{PF}{}^{(-)}\psi_{j_2l_2m_2}\,|\,V_{PN}$$
$$\times|\,\psi_{j_1l_1m_1}\Psi_{DI}{}^{(+)}\rangle|^2. \quad (4a)$$

This last expression is valid for single (l_1j_1) and (l_2j_2) configurations. The ψ_{jlm}'s are the spatial part of the single-particle wave functions:

$$\phi_{ljm_j}=\sum_{m\nu}(l\tfrac{1}{2}m\nu\,|\,jm_j)\psi_{jlm}\chi_N{}^{\frac{1}{2}\nu}. \quad (4b)$$

$\chi_N{}^{\frac{1}{2}\nu}$ is the spin part of the nucleon wave function. The distorted-wave matrix element for nucleon transfer is given by

$$A_{DF}=\langle\Psi_{PF}{}^{(-)}(\mathbf{r}_{PF})\psi_{j_2l_2m_2}(\mathbf{r}_{NI})\,|\,V_{PN}(\mathbf{r}_{PN})$$
$$\times|\,\psi_{j_1l_1m_1}(\mathbf{r}_{PN})\Psi_{DI}{}^{(+)}(\mathbf{r}_{DI})\rangle \quad (5)$$
$$\approx\left(\frac{M_D}{M_P}\right)^3\int d^3r_{NI}\int d^3r_{DI}\Psi_{PF}{}^{(-)*}\left(\frac{M_I}{M_F}\mathbf{r}_{DI}\right)$$
$$\times\psi_{j_2l_2m_2}{}^*(\mathbf{r}_{NI})V_{PN}\left[\frac{M_D}{M_P}(\mathbf{r}_{DI}-\mathbf{r}_{NI})\right]$$
$$\times\psi_{j_1l_1m_1}\left[\frac{M_D}{M_P}(\mathbf{r}_{DI}-\mathbf{r}_{NI})\right]\Psi_{DI}{}^{(+)}(\mathbf{r}_{DI}), \quad (6)$$

where the "no-recoil" approximation

$$\mathbf{r}_{AF}=\frac{M_I}{M_F}\mathbf{r}_{DI}+M_N\left(\frac{M_F+M_P}{M_FM_D}\right)\mathbf{r}_{PN}\approx\frac{M_I}{M_F}\mathbf{r}_{DI} \quad (7)$$

has been made in $\Psi_{PF}{}^{(-)}$. $\mathbf{r}_{XY}$ is the relative position vector between particles X and Y. By means of the finite-range formalism of Sawaguri and Tobocman,[4]

TABLE II. Optical parameters. The same optical parameters were used in both the initial and final channel for each reaction.

	^{10}B(^{14}N, ^{13}N)^{11}B	^{27}Al(^{16}O, ^{15}N)^{28}Si	^{11}B(^{16}O, ^{15}N)^{12}C (g.s.) No core	^{11}B(^{16}O, ^{15}N)^{12}C (g.s.) Repulsive core	^{11}B(^{16}O, ^{15}N*(6.33))^{12}C Weak core	^{11}B(^{16}O, ^{15}N*(6.33))^{12}C Repulsive core
V	50.0	50.0	20.0	20.0	20.0	20.0
W	10.0	10.0	8.0	5.0	5.0	5.0
r_0	1.15	1.25	1.25	1.25	1.25	1.25
a	0.55	0.55	0.50	0.50	0.50	0.50
V_s	0.0	0.0	0.0	−100.0	−50.0	−100.0
W_s	0.0	0.0	0.0	10.0	10.0	10.0
r_{0s}	...	...	...	0.0	0.0	0.0
a_s	...	...	...	1.0	0.5	1.0

the matrix element can be expressed as follows:

$$A_{DF}\approx\sum_{LM}\langle\Psi_{PF}^{(-)}\left(\frac{M_I}{M_F}\mathbf{r}\right)\mid Y_L{}^M(\Omega)F_{LM}(r)\mid\Psi^{(+)}(\mathbf{r})\rangle, \tag{8a}$$

where

$$F_{LM}(r)=\sum_n \mathfrak{F}_n{}^L(2,\beta r)\mathfrak{I}^{LMn}(1,\beta_1;1,\beta_2). \tag{8b}$$

$$\mathfrak{I}^{LMn}(1,\beta_1;1,\beta_2)=\left(\frac{M_D}{M_p}\right)^3\sum_{s_2n_2}G_{l_1n_1}{}^{PN}(1,\beta_1)G_{l_2n_2}{}^{NI*}(1,\beta_2)\times\begin{Bmatrix}l_2&m_2\\l&m\\l_1&m_1\end{Bmatrix}\begin{Bmatrix}s_1&n_1&l_1&\beta_1&1\\s_2&n_2&l_2&\beta_2&1\\&n&l&\beta&\end{Bmatrix}, \tag{8c}$$

$$s_1=n-s_2-\tfrac{1}{2}(l_1+l_2-l), \tag{8d}$$

$$0\leq s_1\leq n_1,\qquad 0\leq s_2\leq n_2, \tag{8e}$$

$$\beta=[\beta_1{}^2\beta_2{}^2/2(\beta_1{}^2+\beta_2{}^2)]^{1/2}. \tag{8f}$$

$$\begin{Bmatrix}l_2&m_2\\l&m\\l_1&m_2\end{Bmatrix}=i^{(l_2-l-l_1)}\times 8\left[\frac{(2l+1)(2l_1+1)}{4\pi(2l_2+1)}\right]^{1/2}\times(ll_1mm_1\mid l_2m_2)(ll_100\mid l_20), \tag{8g}$$

and

$$\begin{Bmatrix}s_1&n_1&l_1&\beta_1&1\\s_2&n_2&l_2&\beta_2&1\\&n&l&\beta&\end{Bmatrix}=4\beta^3(\pi/3)^{3/2}\times\frac{(2\beta)^{2n-l}}{\beta_1{}^{2s_1+l_1}\beta_2{}^{2s_2+l_2}}(-1)^{n_1+n_2-s_1-s_2}\times\frac{[n!\Gamma(n+l+\frac{3}{2})n_1!\Gamma(n_1+l_1+\frac{3}{2})n_2!\Gamma(n_2+l_2+\frac{3}{2})]^{1/2}}{s_2!(n_2-s_2)!\Gamma(s_2+l_2+\frac{3}{2})s_1!(n_1-s_1)!\Gamma(s_1+l_1+\frac{3}{2})}, \tag{8h}$$

$$G_{l_1n_1}{}^{PN}(1,\beta_1)=\int_0^\infty r^2dr\,V_{PN}\left(\frac{M_D}{M_P}r\right)\times R_{j_1l_1}\left(\frac{M_D}{M_P}r\right)\mathfrak{F}_{n_1}{}^{l_1}(1,\beta,r), \tag{8i}$$

and

$$G_{l_2n_2}{}^{NI}(1,\beta_2)=\int_0^\infty r^2dr\,R_{j_2l_2}(r)\mathfrak{F}_{n_2}{}^{l_2}(1,\beta_2r). \tag{8j}$$

$R_{j_il_i}$ is the radial part of the single-particle wave function,

$$\psi_{j_il_im_i}=Y_{l_i}{}^{m_i}R_{j_il_i}\qquad(i=1,2). \tag{8k}$$

$\mathfrak{F}_n{}^l(1,\beta r)$ is the radial harmonic-oscillator function, and

$$\mathfrak{F}_n{}^l(2,\beta r)=e^{-\frac{1}{2}\beta^2r^2}\mathfrak{F}_n{}^l(1,\beta r). \tag{8l}$$

L is the orbital-angular-momentum transfer.

These expressions easily give the following expression for the cross section:

$$\frac{d\sigma}{d\Omega}=\frac{m_im_f}{(2\pi\hbar^2)^2}\frac{k_D}{k_P}\frac{(2J_F+1)}{(2J_I+1)}B\times\sum_{LM}\frac{|\langle\Psi_{PF}^{(-)}\mid Y_{LM}F_{LM}\mid\Psi_{DI}^{(+)}\rangle|^2}{2L+1}, \tag{9a}$$

where

$$B=n_Dn_F(\theta_{j_1l_1}{}^{(1)}\theta_{j_2l_2}{}^{(2)}4\{[(2l_1+1)(2l_2+1)]^{1/2}/\pi\}\times W(l_2j_2l_1j_1;\tfrac{1}{2}L)(l_2l_100\mid L0))^2. \tag{9b}$$

n_D and n_F are the number of identical particles in the initial projectile and final target, respectively, that may be transferred. They arise from antisymmetrization of the wave function which produces several contributing direct amplitudes.[3]

Spectroscopic factors may be defined by $S_1=n_D[\theta_{j_1l_1}{}^{(1)}]^2$ and $S_2=n_F[\theta_{j_2l_2}{}^{(2)}]^2$. In order to compare the magnitudes of the cross sections with experiment, the spectroscopic factors used in this paper are primarily simple shell-model values. However, the values for the ^{10}B(^{14}N, ^{13}N)^{11}B reaction were taken from Goldfarb and Steed.[10] $\theta_{j_il_i}{}^{(i)}$ $(i=1,2)$ is 1 when an overlap is taken between a closed shell and a closed shell plus or minus a particle. In this case, S_i equals the number of identical particles n_D or n_F (Table I).

Table I gives the single-particle transition assumed for each reaction along with the orbital-singular-momentum transfer L for each reaction. L is severely limited by the two triangle relationships, $\Delta(l_1l_2L)$ and $\Delta(j_1j_2L)$, and by parity, $(-1)^{l_1+l_2+L}=+1$.

The bound-state wave functions were computed in a Woods-Saxon potential with a diffuseness $a=0.55$ F for all reactions. A radius $r_0=1.25$ F ($R=r_0\times A^{1/3}$) was used in all cases except for the ^{10}B(^{14}N, ^{13}N)^{11}B reaction for which $r_0=1.15$ F was used. The latter value was used to facilitate a comparison with Ref. 10.

The optical potentials used have the form

$$V_{\text{opt}}=-(V+iW)[1+e]^{-1}-4(V_s+iW_s)d/dr[1+e_s]^{-1} \tag{10a}$$

with

$$e=\exp[(r-R)/a]\text{ and }e_s=\exp[(r-R_s)/a_s], \tag{10b}$$

$R=r_0\times A^{1/3}$. In order to reduce the number of free parameters, the optical parameters were arbitrarily chosen to have the same values in the initial and final channels. The values are displayed in Table II.

---

[10] L. J. B. Goldfarb and J. W. Steed, Nucl. Phys. **A116**, 321 (1968).

TABLE III. Reaction variables: $E_{c.m.}$ is the center-of-mass energy for incident channel; E_c is the Coulomb barrier energy in center of mass; $D_{min}=2\eta/k$, where η and k are the average Coulomb constant and wave number for incident and final channels; $R=r_0(A_1^{1/3}+A_2^{1/3})$.

Reaction	E_{lab}	Q	$E_{c.m.}$	E_c	$\bar{D}_{min}$	R	r_0
$^{10}B(^{14}N, ^{13}N)^{11}B$	9.0	0.913	3.75	7.7	10.4	5.3	1.15
$^{10}B(^{14}N, ^{13}N)^{11}B$	16.0	0.913	6.67	7.7	7.9	5.3	1.15
$^{27}Al(^{16}O, ^{15}N)^{28}Si$	30.0	−0.545	18.84	18.8	7.9	6.9	1.25
$^{27}Al(^{16}O, ^{15}N)^{28}Si$	36.0	−0.545	22.6	18.8	7.2	6.9	1.25
$^{11}B(^{16}O, ^{15}N)^{12}C$	30.0	3.845	12.2	8.5	4.2	5.9	1.25
$^{11}B(^{16}O, ^{15}N^*)^{12}C$	30.0	−2.49	12.2	8.5	5.4	5.9	1.25

III. RESULTS

Table III compares in two ways the scattering regions being studied by the three reactions: First, by the value of the incident energy in the center-of-mass frame and second by the classical distance of closest approach, $\bar{D}_{min}$, for two particles following a Coulomb trajectory for 180° scattering $\bar{D}_{min}=2(\bar{n}/\bar{k})$. $\bar{n}$ is the average Coulomb constant for initial and final channels. $\bar{k}$ is the average wave number. For the $^{10}B(^{14}N, ^{13}N)^{11}B$ reaction the incident energy is well below the Coulomb barrier, and $\bar{D}_{min}$ is much greater than the radius R for which the two ions just touch. For the $^{27}Al(^{16}O, ^{15}N)^{28}Si$ reaction, the incident energy is comparable to the Coulomb barrier, and $\bar{D}_{min}$ is slightly larger than R. For this reaction, distorting effects of the optical potential begin to be important. Finally, for the $^{11}B(^{16}O, ^{15}N)^{12}C$ reaction, the energy is above the Coulomb barrier, and the ions would experience classical overlap if they simply followed classical Coulomb trajectories. $\bar{D}_{min}$, which is an average value for incident and exit channels, is smaller for the ground-state transition than it is for the excited-state transition since the final kinetic energy is larger for the ground-state transition. The ground-state transition, therefore, is more sensitive to optical-model parameters.

A. $^{10}B(^{14}N, ^{15}N)^{11}B$

Goldfarb and Steed[10] have studied this reaction by means of an approximate DWBA theory for incident energies from 9.0 to 16.0 MeV. At the low energies, they extracted spectroscopic factors in agreement with earlier results, reproduced the experimental energy dependence of the total cross section, and obtained reasonable fits to the angular distributions. At the higher energies, where the effects of optical distortion appear, the theoretical cross sections were too large and the fits to the angular distributions were poorer. Our calculations agree with their results at the lower energies. At the higher energies, an absorptive potential ($V=50.0$, $W=10.0$ MeV) removed the discrepancy in the total cross section and also improved the fit to the angular distributions (see Figs. 1 and 2). The results were not sensitive to the exact values of the optical-potential strengths, even at the highest energy ($E=16.0$ MeV). For instance, an increase in W from 10.0 to 19.0 MeV produced only an 8% decrease in the total cross section. As noted by Goldfarb and Steed, the total cross section is very sensitive to the parameters of the bound neutron since the cross section depends primarily on the asymptotic behavior of the bound-state wave function. Also, as noted by them, the magnitude of the experimental angular distributions is inconsistent with the total cross section which was measured in a different experiment. While we obtain agreement with the total cross section with a spectroscopic factor of $S=1.1$, the theoretical angular distributions have been multiplied by an additional factor of 2.3.

B. $^{27}Al(^{16}O, ^{15}N)^{28}Si$

The transitions in this reaction to both the ground and first excited state at 1.78 MeV in ^{28}Si have been

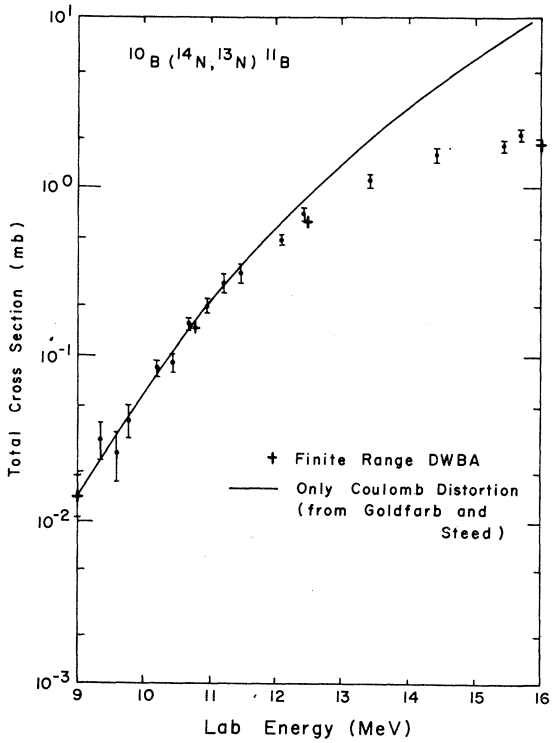

FIG. 1. Energy dependence of total cross section for $^{10}B(^{14}N, ^{13}N)^{11}B$.

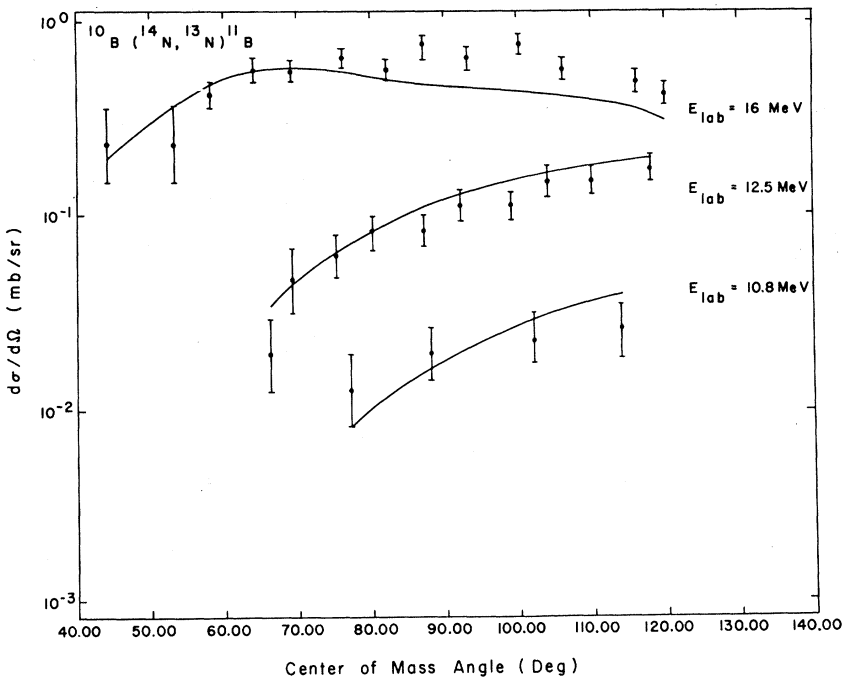

FIG. 2. Anguar distributions for $^{10}B(^{14}N, ^{13}N)^{11}B$.

successfully studied by Dar's diffraction theory.[2] With a smooth cutoff he is able to fit angular distributions for both transitions at incident energies of 28.5, 30.0, and 36.0 MeV. Our DWBA calculations also give reasonable fits to the experimental angular distributions. One interesting difference between the two calculations is the introduction of an apsidal distance R for the diffraction theory which determines the location of the diffraction peak. For the ^{27}Al-^{16}O reaction $r_0 \sim 2.0$ F, where $R = r_0 \times (A_1^{1/3} + A_2^{1/3})$. However, in the DWBA picture the radius of the optical potential should be directly related to the physical size of the nuclei. In that case, a more usual $r_0 \sim 1.2$ F gives a diffraction peak at the correct angle.

The diffraction peaks could be reproduced with widely varying sets of optical-potential strengths. In particular, both sets ($V = 50.0$, $W = 10.0$ MeV) and ($V = 10.0$, $W = 2.0$ MeV) gave fair results. The former gave the better fit (Fig. 3). The energy dependence of the total cross section differed radically, however, for the two sets (see Table IV). For the first set the energy excitation function was relatively constant. For the second set, the excitation function was a rapidly increasing function, and the total cross section was too large in magnitude unless a large reduction of the single-particle spectroscopic factors is assumed. Since the experimental excitation function for the ground-state transition increases at first and then levels out, optical parameters intermediate between the two above sets are suggested.

TABLE IV. Total cross sections for $^{27}Al(^{16}O, ^{15}N)^{28}Si$ (g.s.).

Energy (MeV)	Total cross section (mb) $V=50.0$ $W=10.0$	$V=10.0$ $W=2.0$	Expt
28.5	1.63	7.9	0.80
30.0	1.63	14.8	1.35
36.0	1.57	48.0	1.37

A calculation has also been made for the 1.78-MeV first-excited-state transition at 30.0-MeV incident energy. The fit to the experimental angular distribution was reasonable. The same optical parameters were used as for the ground-state transition, and it was assumed that the proton was stripped into the $2s_{1/2}$ state. The resulting theoretical cross section was $\sim 35\%$ high. Since the 1.78-MeV state is a rotational state and not of single-particle character, one should expect the theoretical value to be high. However, since the optical parameters are uncertain the calculated magnitude has little significance.

In this reaction, the results begin to exhibit some sensitivity to optical-model parameters, and a calculation was made to check for effects of a repulsive core. This was done by setting $R_s = 0$ in the surface term of the optical potential. This procedure gives a term of the form

$$V_{\text{core}} = -(V_s + iW_s)[1/\cosh^2(r/2a_s)].$$

With $V_s = -100.0$ MeV, $W_s = 5.0$ MeV, and $a_s = 1.0$ F, the effect of the core for the ground-state transition was to increase the cross section by $\sim 20\%$ and to shift the diffraction peak to the right $\sim 10°$. These effects

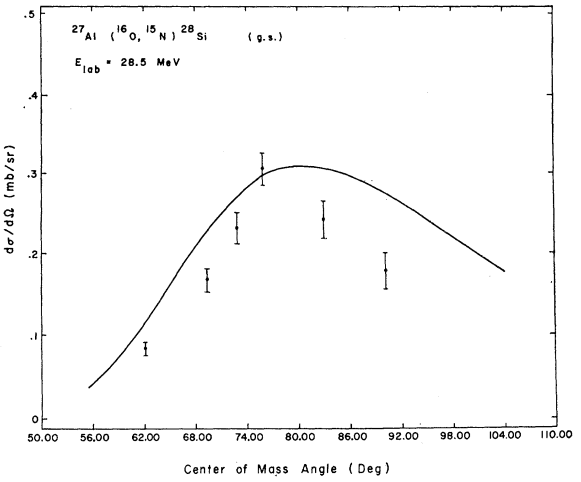

(a)

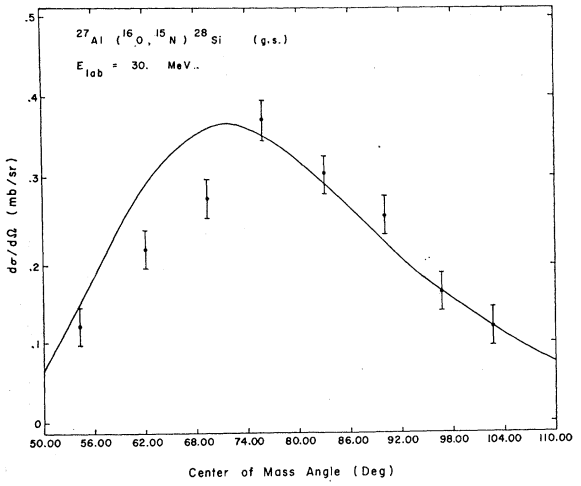

(b)

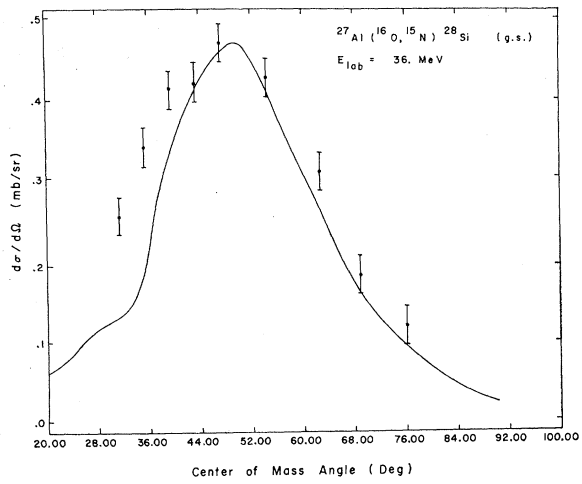

(c)

FIG. 3. Angular distributions for ^{27}Al(^{16}O, ^{15}N)^{28}Si (g.s.).

could be absorbed, however, by changing other parameters in the optical potential.

C. ^{11}B(^{16}O, ^{15}N)^{12}C

This reaction has been investigated at 30.0-MeV incident energy for both the ground-state transition and for the transition which leaves ^{15}N in its third excited state at 6.33 MeV. Since this energy region is definitely above the Coulomb barrier, the angular distributions become very sensitive to the optical-model parameters. These transitions have also been analyzed by Dar and Kozlowsky[11] with the diffraction model. They interpret the angular distribution for the excited-state transition as consisting of two diffraction peaks: a forward peak due to proton transfer and a backward peak due to α-particle transfer in the reaction ^{11}B(^{16}O, ^{12}C)^{15}N. Although the angular distribution for the ground-state transition is more complicated, a similar interpretation is given for it.

For these transitions the DWBA results were less conclusive. First, the over-all fits were poorer and, second, there was generally not a clear basis to select optimum parameters. Nevertheless, a number of points can be made (the best fits are shown in Figs. 4 and 5):

TABLE V. Magnitude of cross sections for ^{11}B(^{16}O, ^{15}N)^{12}C. Maximum value of angular distributions for ^{11}B(^{16}O, ^{15}N)^{12}C ground- and excited-state transitions.

	$(d\sigma/d\Omega)_{max}$ (mb/sr)		
	DWBA Weak or no core	Repulsive core	Expt
Ground state	2.78	9.18	1.5
Excited state	2.41	2.05	0.48

(1) The fits were better for the excited-state transitions.

(2) A repulsive core enhanced both transitions for angles greater than 100°. Only for the excited-state transition was the enhancement sufficient to agree with experiment. For smaller angles in the ground-state transition, the core strongly affected the cross section but not in a predictable fashion.

(3) The DWBA could reproduce oscillations near 70° in the ground-state transition, which the diffraction model could not, but no over-all improvement was attained.

(4) In a qualitative sense, the DWBA agreed with the diffraction model only if either a cutoff radius was introduced or the absorptive part of the potential was large (~10 MeV).

[11] A. Dar and B. Kozlowsky, Phys. Rev. Letters **15**, 1036 (1965).

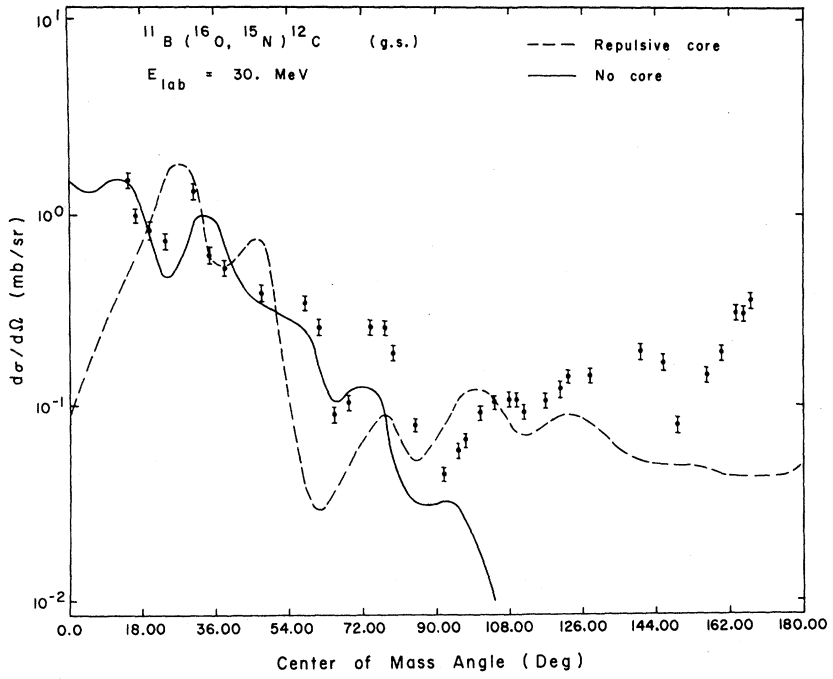

FIG. 4. Angular distributions for $^{11}B(^{16}O, ^{15}N)^{12}C$ (g.s.).

(5) The total cross sections are of the right order of magnitude but are not well determined enough to extract spectroscopic factors (Table V).

(6) In order to test the possibility of α transfer in the DWBA picture, a calculation was made for the excited-state transition. It was assumed that an s-state α particle was stripped from ^{16}O into an s state of ^{11}B to produce the excited state in ^{15}N with an over-all spectroscopic factor of 1. The total cross section obtained was between one and two orders of magnitude too small, and the angular distributions oscillated rapidly in complete disagreement with experiment.

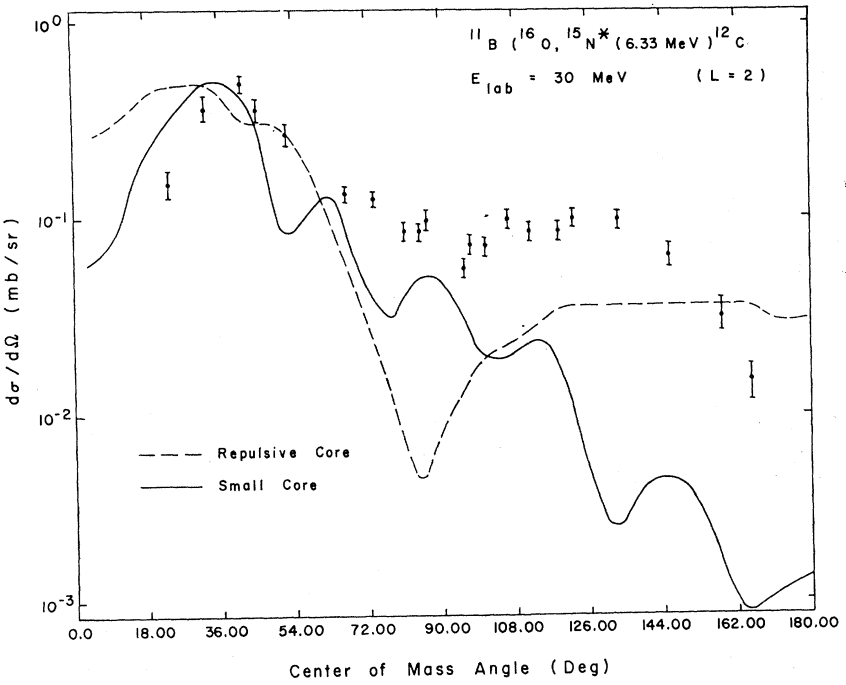

FIG. 5. Angular distributions for $^{14}B(^{16}O, ^{15}N^*(6.33\ MeV))^{12}C$.

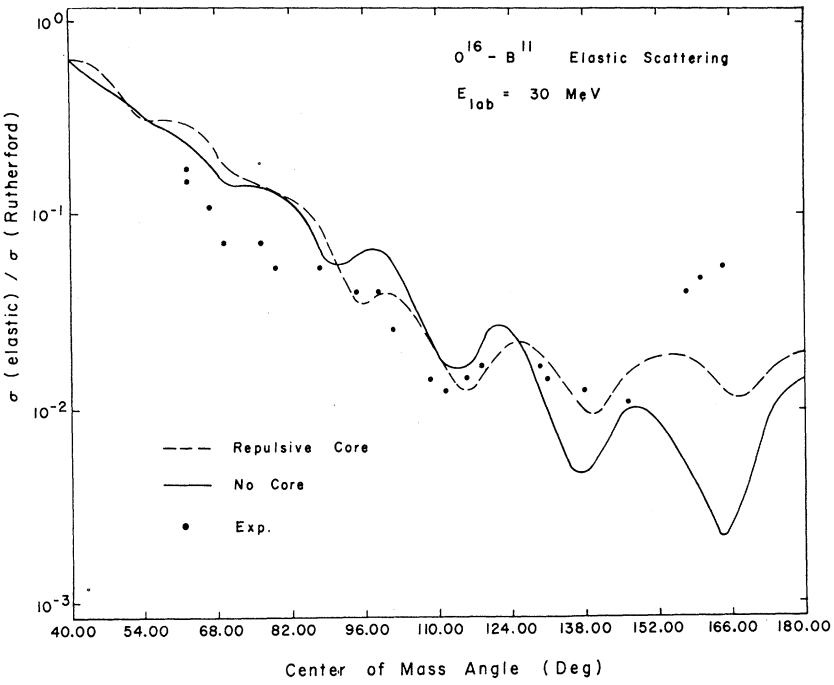

FIG. 6. Elastic scattering for ^{16}O-^{11}B.

These conclusions are weakened by the fact that the relatively heavy mass of the transferred α particle may make neglected recoil effects important.

Elastic data for ^{11}B-^{16}O scattering at 30.0 MeV has been reported along with an analysis by Bock *et al.*[8] We have also analyzed these data in an effort to obtain optical-model parameters independently of the reaction calculations. Potentials with and without a repulsive core were tried. Neither set gave a good fit, and there was little basis for choosing between them (Fig. 6). The potentials obtained were not unique but were consistent with the potentials used for the reaction studies. Bock *et al.* used potentials with a real depth of 70.0 MeV. Guided by other efforts[9,12] in which shallower potentials have been suggested, we have found that the shallower wells produce fits comparable to those obtained from the deeper potentials. Also, the reaction angular distributions favor the shallower wells.

IV. CONCLUSIONS

At energies near and below the Coulomb barrier, the theory provides a reliable means to calculate angular distributions and extract spectroscopic factors. There are no restrictions placed on the calculations due to nonzero Q values or because the transferred particle is charged. At these same energies, the results agree with the tunneling and diffraction theories.

For energies above the Coulomb barrier, increased sensitivity of the results to the optical potential provides a test of these parameters. However, the single example presented here was inconclusive. A more comprehensive study is needed in which one determines optical parameters from the elastic data and then does the reaction calculation with the predetermined parameters.

The central role of the optical potential at the higher energies gives additional incentive for its study by other means. A nonlocality, for example, would give rise to a Perey effect[13] known to be important for nucleon-nucleus reactions. The results are sensitive to a repulsive core and could shed light on its importance in a broader survey of data.

Polarization of the colliding ions and recoil effects may also have eventual importance.

[12] R. H. Siemssen, J. V. Maher, A. Weidinger, and D. A. Bromely, Phys. Rev. Letters **19**, 369 (1967).

[13] F. G. Perey, in *Direct Interactions and Nuclear Reaction Mechanisms*, edited by E. Clementel and C. Villi (Gordon and Breach Science Publishers, Inc., New York, 1963), p. 125.